ACS Energy LETTERS

Cite This: ACS Energy Lett. 2019, 4, 2975−2982

http://pubs.acs.org/journal/aelccp

LETTER

Tuning Emission and Electron−Phonon Coupling in Lead-Free Halide Double Perovskite $Cs_2AgBiCl_6$ under Pressure

Long Zhang,[†] Yuanyuan Fang,[†] Laizhi Sui,[‡] Jiejuan Yan,[§] Kai Wang,*[,†,§] Kaijun Yuan,[‡] Wendy L. Mao,[§,∥] and Bo Zou*[,†]

[†]State Key Laboratory of Superhard Materials, College of Physics, Jilin University, Changchun 130012, China

[‡]State Key Laboratory of Molecular Reaction Dynamics, Dalian Institute of Chemical Physics, Chinese Academy of Sciences, 457 Zhongshan Road, Dalian 116023, China

[§]Department of Geological Sciences, Stanford University, Stanford, California 94305, United States

[∥]Stanford Institute for Materials and Energy Sciences, SLAC National Accelerator Laboratory, Menlo Park, California 94025, United State

Supporting Information

ABSTRACT: **Lead-free halide double perovskites have been proposed as candidates to replace Pb-halide perovskites in photovoltaic and optoelectronic applications due to their enhanced stability and nontoxicity. However, the limited understanding of the fundamental properties of halide double perovskites represents a hurdle to further improvement of their device performance. Our experimental studies demonstrate that the broad emission of $Cs_2AgBiCl_6$ with a large Stokes shift stems primarily from exciton self-trapping owing to strong electron−phonon coupling. An unusual blue shift of the emission accompanied by a red shift of the absorption edge occurred due to the reduced lattice relaxation energy upon lattice compression in the cubic phase. Electron−phonon coupling reduction is critical to the enhancement of photoluminescence intensity and tuning emission range in $Cs_2AgBiCl_6$ under high pressure. The structure−property relationships illuminated by our work can provide the basis for improving the performance of halide double perovskites.**

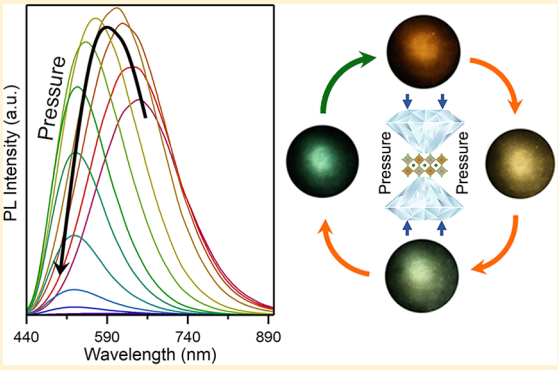

Due to their excellent properties including strong light absorption, long carrier diffusion lengths and lifetimes, high charge carrier mobility, suitable band gap, etc.,[1−3] metal halide perovskites have attracted considerable attention from the clean energy sector for future photovoltaic and optoelectronic applications. Despite the performance and exciting potential of Pb-based perovskites, the environmental impact and toxicity of Pb and the inherent instability of the pristine materials with respect to moisture, heat, oxygen, and light are still primary concerns that severely limit their commercialization and the widespread use of this new technology.[4,5]

Substantial efforts have been invested in the search for low-toxicity and stable halide perovskites with photovoltaic and photoelectric properties that are comparable to those of Pb-based perovskites. Recently, Bi-based halide double perovskites Cs_2AgBiX_6 (Br, Cl) have been proposed and synthesized as promising alternatives. These perovskites possess three-dimensional (3D) cubic structures with corner-sharing metal halide octahedra and considerable flexibility for compositional adjustments.[6−10] Halide double perovskites exhibit great potential for a multitude of other applications, such as photodetectors, X-ray detectors, photocatalysts, light-emitting diodes (LEDs), etc.[11−14] Even though numerous investigations have been performed to improve device performance, the optimized PCE of halide double perovskite photovoltaic devices (<2.5%) is still lower than that of the Pb-based perovskite analogues,[15−17] implying inherent electronic limitations and differences compared to Pb-containing materials. Strong electron−phonon coupling is found in halide double perovskite,[18,19] which increases carrier scattering and reduces charge carrier mobility, low photoluminescence (PL) quantum yield, and undesirable electron−hole recombination.[8,20,21]

Received: October 1, 2019
Accepted: November 13, 2019
Published: November 13, 2019

Downloaded via DALIAN INST OF CHEMICAL PHYSICS on July 22, 2020 at 02:55:33 (UTC).
See https://pubs.acs.org/sharingguidelines for options on how to legitimately share published articles.

© 2019 American Chemical Society

DOI: 10.1021/acsenergylett.9b02155
ACS Energy Lett. 2019, 4, 2975−2982

Whether the emission mechanisms of halide double perovskites stem from indirect transitions, defects, or exciton self-trapping remains a subject of debate.[18,22,23] Various strategies are needed to further understand and modify their electronic structures and relevant properties, including the band gap, electron−phonon interactions, the emission mechanism, and the electric transport of halide double perovskites.[24]

The atomic-level understanding of structure−property relationships can provide crucial insight into materials development and improved performance. High-pressure technology is a powerful tool for modifying the lattice structures and electronic wave functions of materials, which in turn alters their various physical/chemical properties without changing chemistry.[25] In recent years, high-pressure studies on conventional halide perovskites (ABX_3) have been conducted to improve their photovoltaic properties and reveal novel phenomena, including band gap narrowing, carrier lifetime increase, PL enhancement, resistance reduction, etc.[26−32] Band gap narrowing and an increase in carrier lifetime in methylammonium lead iodide ($MAPbI_3$) can occur simultaneously under mild pressure (<0.3 GPa), which is promising for practical applications. Under higher pressure, the metallization of $MAPbI_3$ by band gap closure was confirmed above 60 GPa, indicateing a wholly new electronic structure and transport properties.[33] The partially retained band gap narrowing of the pressure-treated 2D hybrid perovskite $(C_4H_9NH_3)_2(CH_3NH_3)_{n-1}Pb_nI_{3n+1}$ and 3D halide double perovskite $Cs_2AgBiBr_6$ by achieving metastable states offers a practical approach to tailor their optoelectronic properties for improved light absorbers.[34,35]

Here, we systematically studied the optical, electrical, and structural properties of $Cs_2AgBiCl_6$ with applied pressure up to 31 GPa at room temperature by conducting in situ high-pressure PL, UV−vis absorption, X-ray diffraction, Raman, and resistance experiments. We confirmed that the broad emission of $Cs_2AgBiCl_6$ mainly originates from exciton self-trapping. A negative shift of PL relative to the absorption edge was observed due to the decreased lattice relaxation energy upon compression. Bond length compression remarkably reduced electron−phonon coupling and suppressed ionic transport in the cubic phase of $Cs_2AgBiCl_6$. This work not only reveals the structure−property relationships in halide double perovskites but also clarifies potential engineering routes for considerably modifying the crystal structures and various properties of halide double perovskite with better materials by design.

Pressure effects on optical properties, including the band gap and emission by tuning the bond length and bond angle in crystals, are of great concern to us for photovoltaic or optoelectronic applications. To determine how the band gap of $Cs_2AgBiCl_6$ changes with compression, we performed in situ high-pressure UV−vis absorption measurements up to ca. 31 GPa (Figure 1). $Cs_2AgBiCl_6$ displayed a sharp increase in absorption below 440 nm with a gentle absorption tail at ambient conditions, suggesting indirect band gap character, which is consistent with previous experimental and theoretical reports.[23] The band gap of $Cs_2AgBiCl_6$ was estimated by extrapolating the linear portion of the $(\alpha dh\nu)^{1/2}$ versus $h\nu$ in indirect band gap Tauc plots, where α is the absorption coefficient, d is the sample thickness, and $h\nu$ is the photon energy (Figure 1b). The pressure-driven band gap evolution of $Cs_2AgBiCl_6$ upon compression is shown in Figure 1c. As pressure increases, the band gap of $Cs_2AgBiCl_6$ gradually red shifts below 5 GPa, followed by a sharp increase above 5 GPa

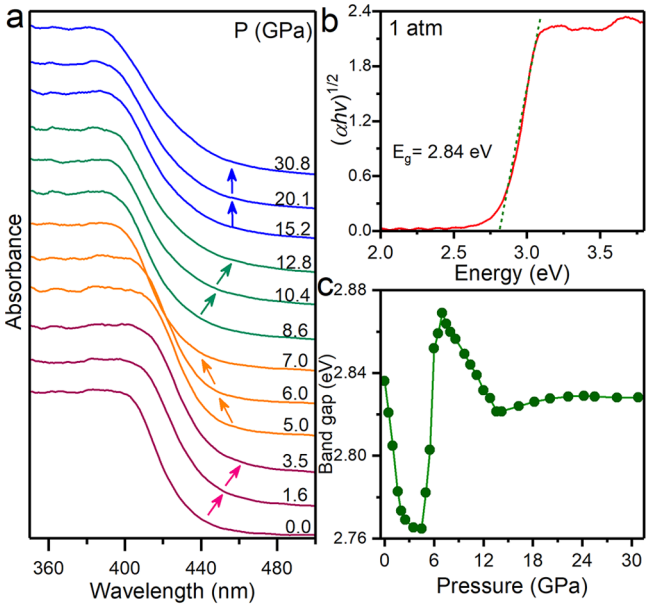

Figure 1. (a) Absorption spectra of $Cs_2AgBiCl_6$ as a function of pressure. The arrows trace the evolution of the absorption edge. (b) Indirect band gap Tauc plot for $Cs_2AgBiCl_6$ at ambient pressure. (c) Band gap evolution of $Cs_2AgBiCl_6$ as a function of pressure.

over a small pressure region. With the further increase of pressure above 7 GPa, a red shift in the band gap is observed. When the applied pressure reaches approximately 14 GPa, the band gap is nearly unchanged until ca. 31 GPa. During decompression, the absorption spectra of $Cs_2AgBiCl_6$ maintain a blue shift above 0.8 GPa. When the pressure is released completely, the absorption spectra of pressure-treated samples show a slight difference compared with its initial state (Figure S1).

We carried out in situ high-pressure PL experiments to explore the light emission behavior of $Cs_2AgBiCl_6$ as a function of pressure (Figure 2). Under ambient pressure, $Cs_2AgBiCl_6$ exhibits a broad orange emission with a peak centered at 648 nm and a full width at half-maximum (fwhm) of 186 nm, suggesting a very large Stokes shift of 265 nm (Figures 2b and S2). As the pressure increases, the PL peak evidently blue shifts along with the PL peak position from an initial 648 to 532 nm at 5.1 GPa and then slowly red shifts (Figure 2c), corresponding to a change of carrier lifetime from a continuous decrease to slow increase (Figures S3 and S4). Meanwhile, the corresponding fwhm of the PL spectrum shows a remarkable decrease before 5.1 GPa, followed by widening upon further compression (Figure 2d). The dramatic behavior of the negative shift of the PL peak toward higher energy relative to the absorption edge is distinctly different from the reported high-pressure studies of conventional Pb-based halide perovskites with a direct transition, implying a different electronic transition mechanism rather than the multiple indirect transitions. Initially, the PL intensity of $Cs_2AgBiCl_6$ increases gradually for pressure below 1 GPa. This occurrence is followed by a progressive decrease in PL until it completely disappears at approximately 8 GPa (Figure 2e). Upon decompression, the PL spectra return to the original profile and position, but the PL intensity is weaker than that of its initial state (Figure S5). This abnormal phenomenon can be reproduced in our repeated experiments. The considerable

DOI: 10.1021/acsenergylett.9b02155
ACS Energy Lett. 2019, 4, 2975−2982

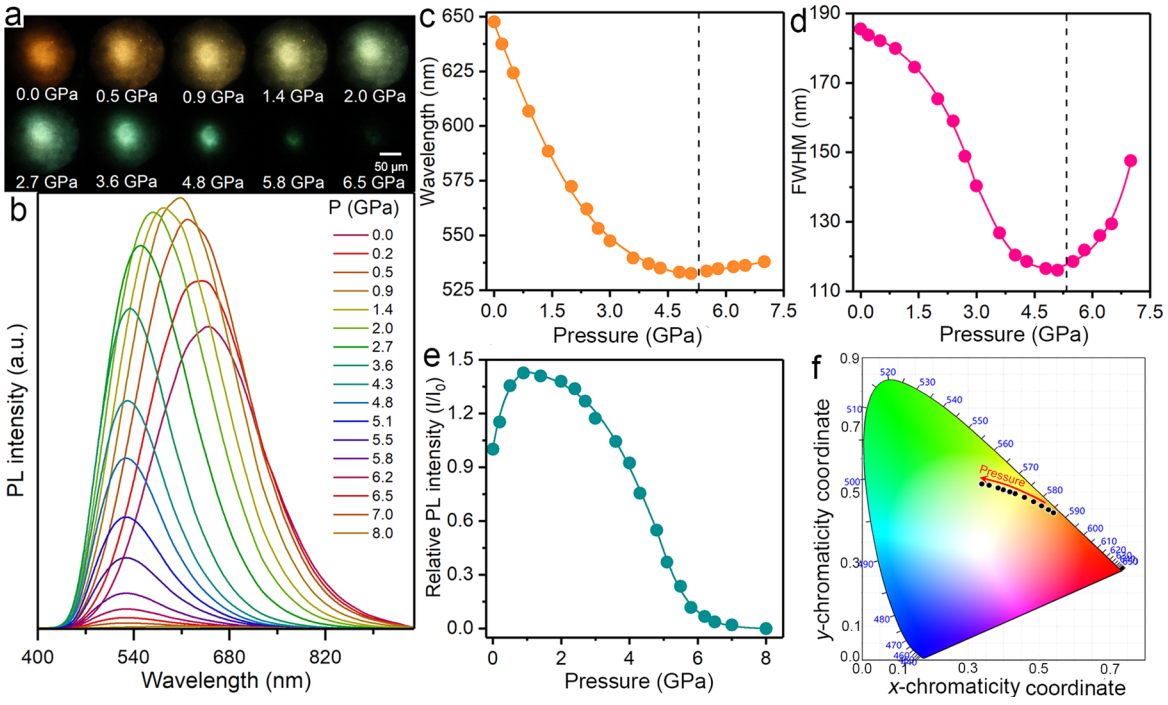

Figure 2. (a) PL micrographs upon compression. (b) PL spectra of $Cs_2AgBiCl_6$ as a function of pressure during compression. (c) PL peak location of $Cs_2AgBiCl_6$ against pressures. (d) Fwhm of $Cs_2AgBiCl_6$ as a function of pressure. (e) Evolution of PL intensity as a function of pressure. (f) Pressure-dependent chromaticity coordinates of the emissions.

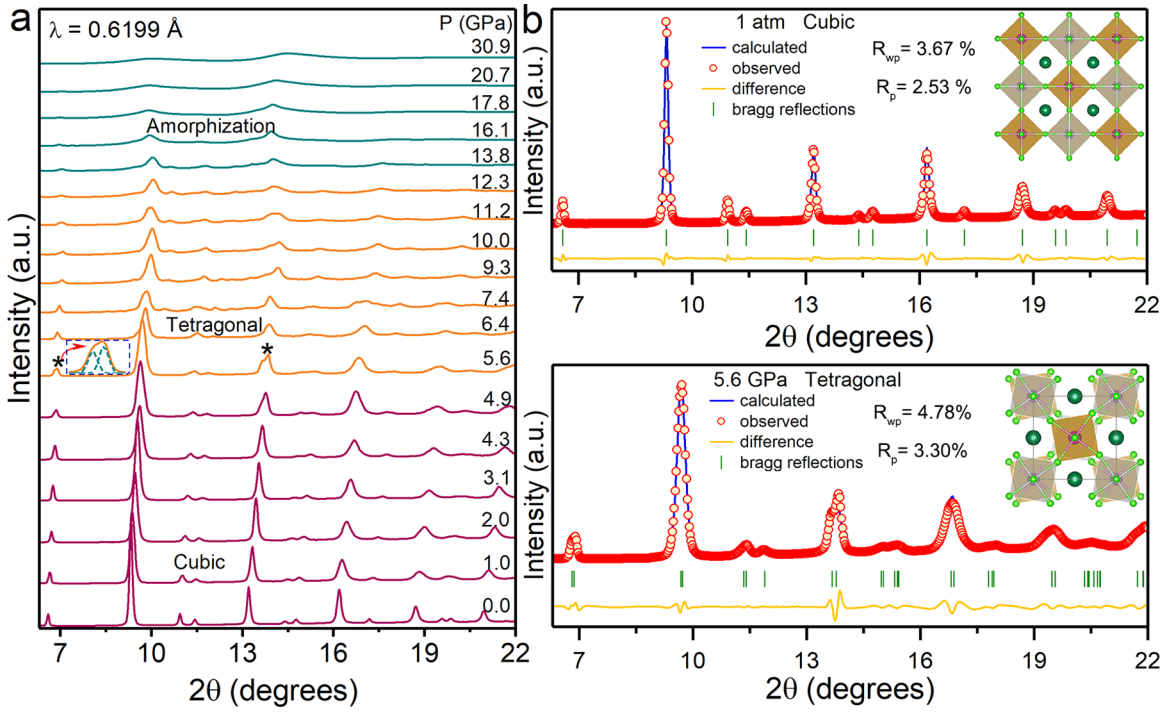

Figure 3. High-pressure synchrotron XRD patterns for $Cs_2AgBiCl_6$. Black asterisks mark the appearance of new diffraction peaks. (b) Rietveld refinement of XRD patterns of $Cs_2AgBiCl_6$ at 1 atm and 5.6 GPa. The insets show the corresponding crystal structure. Cs: dark green ball; Ag: gray ball; Bi: purple ball; Cl: light green ball.

tunability of the PL position, the fwhm, and the intensity for pressure-driven emission spectra indicate continuous changes in the color of light emission with pressure, which can be clearly observed in PL optical images (Figure 2a). Furthermore, we recorded pressure-dependent CIE chromaticity coordinates of emission from $Cs_2AgBiCl_6$ (Figure 2f and Table S1). The evolution of the CIE chromaticity coordinates is continuous from ambient pressure (0.54, 0.44) to 4.8 GPa (0.34, 0.52), corresponding to color transformation from original orange to green-enriched white. The ability to alter emission intensity and chromaticity by high-pressure technologies indicates a prospective strategy for optimizing LED

DOI: 10.1021/acsenergylett.9b02155
ACS Energy Lett. 2019, 4, 2975−2982

design with varying chromaticity for multifunctional applications by using strain/pressure engineering with reasonable chemical regulation or device construction.

The optical properties of $Cs_2AgBiCl_6$ strongly depend on the pressure response of the inorganic lattice framework. To better understand the root cause of the abnormal PL and band gap evolution, we carried out in situ synchrotron high-pressure XRD experiments on $Cs_2AgBiCl_6$ up to ca. 31 GPa at room temperature. Figure 3a shows a series of pressure-dependent XRD patterns. With increasing pressure, the diffraction peaks shift continuously toward smaller *d*-spacing due to lattice compression. At 5.6 GPa, the subtle splitting of two diffraction peaks located at around 6.8 and 13.7° indicates a pressure-induced phase transition,[36] accompanied by the dramatic broadening and weakening of the diffraction peaks with further compression, which should be associated with the deviatoric stress and a transition-induced breakdown of the sample grains originating from the nonhydrostatic conditions according to the previous high-pressure studies.[37,38] As the pressure is increased to 13.8 GPa, significant structural distortion occurs, as evidenced by the disappearance and broadening of partial diffraction peaks, as well as appearance of a broad diffraction background, suggesting the beginning of amorphization and the increased disorder of $AgCl_6$ and $BiCl_6$ octahedra.[39,40] Finally, a complete amorphous phase is observed at around 31 GPa with the disappearance of all sharp diffraction peaks and the presence of only two weak broad bands, indicating a loose long-range order in the crystal structure. During decompression, the amorphous state is preserved before 1.2 GPa, which is obviously lower compared with the onset pressure for amorphization (Figure S6). Finally, $Cs_2AgBiCl_6$ restores to the original cubic phase, but the XRD patterns of pressure-treated samples are broadened and weakened along with the disappearance of partially small diffraction peaks. These findings imply that the crystallinity is not reversible completely after decompression, which should be responsible for changes in optical properties of the pressure-treated samples.

Rietveld refinement was conducted to determine how the crystal structure of $Cs_2AgBiCl_6$ changes with pressure (Figure 3b). At ambient conditions, $Cs_2AgBiCl_6$ possesses a cubic structure with the space group *Fm*-3*m* and lattice parameters a = 10.785(5) Å and V = 1254.470(4) Å^3, in good agreement with previous literature reports.[7] This double perovskite structure is a network of 3D corner-sharing octahedra, where alternating $AgCl_6$ and $BiCl_6$ octahedra are arranged in a rock-salt configuration with Cs atoms occupying the cubic octahedron cavity. The Ag−Cl bond lengths are slightly longer than that of the Bi−Cl bond due to Cl atoms having a small displacement toward Bi atoms. For the 5.6 GPa pattern, a tetragonal structure with the space group *I*4/*m* was adopted to fit two split diffraction peaks. *I*4/*m* is a subgroup of *Fm*-3*m*, allowing $BiCl_6$ and $AgCl_6$ octahedra coherent rotation with an opposite direction along the *c* axis in the *ab* plane. The rotation angle θ of the octahedra in the tetragonal phase is about 7.4°, while the Bi−Cl−Ag bond along the *c* axis remains 180° (Figure S7). In addition, $BiCl_6$ and $AgCl_6$ octahedra are slightly distorted with different Bi(Ag)−Cl bond lengths in the *ab* plane compared with along the *c* axis. Therefore, the cubic−tetragonal transition is primarily dominated by the torsional rotation of $BiCl_6$ and $AgCl_6$ octahedra along the *c* axis with negligible deformation of the $BiCl_6$ and $AgCl_6$ octahedra. The discontinuous cell parameters and volume changes are consistent with optical properties and structural transitions upon compression (Figure S8).

The local lattice vibrations of $Cs_2AgBiCl_6$ are affected by the changes of the inorganic octahedra under pressure; thus, we conducted in situ high-pressure Raman experiments. As shown in Figure 4, we observed three vibrational modes below 360

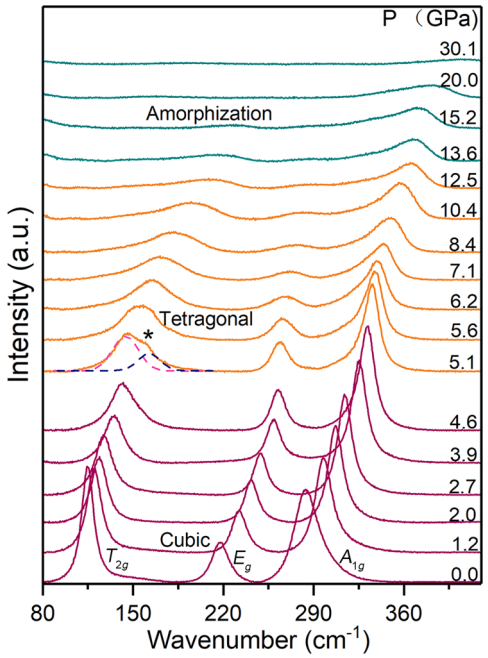

Figure 4. Raman spectra of $Cs_2AgBiCl_6$ as a function of pressure. Black asterisks mark the appearance of new peaks.

cm^{-1} at ambient conditions. According to the assignment of analogues in previous studies, the band at 115 cm^{-1} is ascribed to a breathing vibration of the Ag−Cl bonds with T_{2g} symmetry, while the two bands at 212 and 284 cm^{-1} belong to the stretching vibrations of the $AgCl_6$ octahedron with different vibrational symmetries of E_g and A_{1g}, respectively.[18,19] With increasing pressure, all bands shift to higher frequency owing to the $AgCl_6$ octahedron shrink. As pressure increases to 5.1 GPa, the splitting of the Ag−Cl breathing vibration illustrates the occurrence of a phase transition associated with inorganic octahedron rotation. At above 13.6 GPa, the progressive amorphization of $Cs_2AgBiCl_6$ is observed with the broadening, weakening, and eventual disappearance of the vibrational mode. Upon decompression, all of the Raman shifts are reversible, but the intensity of the vibration mode is relatively weaker than its initial state (Figure S9). Those changes in Raman spectra are consistent with the XRD results.

Electrical conductivity of metal halide double perovskites is a key parameter for their optoelectronic or photovoltaic applications. To track the pressure response on electrical properties of $Cs_2AgBiCl_6$, we implemented in situ resistance experiments upon compression. As shown in Figure S10, $Cs_2AgBiCl_6$ with ionic conduction exhibits poor conductivity, as evidenced by a large resistance. As the pressure increases, the resistance increases continuously before ca. 6 GPa, suggesting that the ionic migration is suppressed due to the reduction of the ionic migration channels along with lattice shrinkage and interstitial spaces reduction.[41,42] Within the tetragonal phase of $Cs_2AgBiCl_6$, the torsional rotations of $BiCl_6$ and $AgCl_6$ octahedra improve the ionic migration channels,

DOI: 10.1021/acsenergylett.9b02155
ACS Energy Lett. 2019, 4, 2975−2982

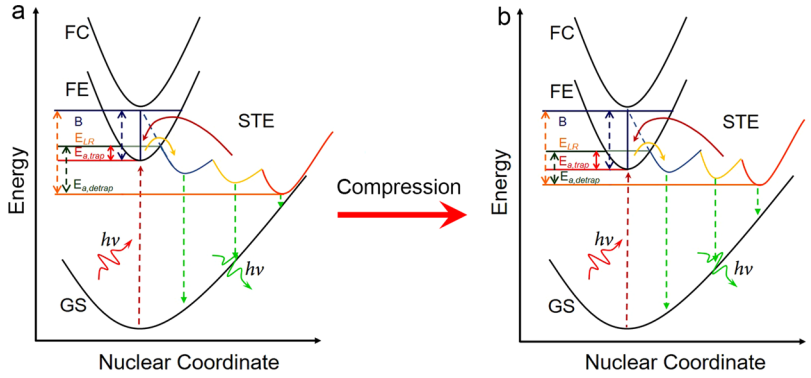

Figure 5. Schematic illustrations of emission evolutions at ambient conditions (a) and high pressure (b) in the cubic phase. Ground state (GS), free-carrier state (FC), free-exciton state (FE), and various self-trapped exciton states (STE), B = half-width of the exciton band, E_{LR} = lattice relaxation energy, $E_{a,trap}$ = activation energy for self-trapping, and $E_{a,detrap}$ = activation energy for detrapping.

which decreases resistance. Under higher pressure, the resistance is almost constant, corresponding to a pressure-induced amorphous phase.

The Fröhlich interactions from the coupling of longitudinal optical (LO) phonons and lattice vibrations are significant scattering mechanisms in polar semiconductors. The A_{1g} LO phonon mode of $Cs_2AgBiCl_6$ has an energy of $\hbar\omega_{LO}$ = 284 cm^{-1} at ambient conditions. The Huang–Rhys parameter S, as an indicator of the electron–phonon coupling strength, allows us to describe the equilibrium position offset between the excited and ground states, as well as the microscopic details of vibration coupling.[43] We can estimate the Huang–Rhys parameters according to the measured Stokes shift energy E_{Stokes} and the LO phonon mode energy according to the relationship $E_{Stokes} = 2S\hbar\omega_{LO}$. At ambient conditions, we obtained a large Huang–Rhys parameter of 18.1, which is slightly larger than the value of the analogues, $Cs_2AgBiBr_6$, which exhibits giant electron–phonon coupling (S = 15.4),[18] indicating a relatively stronger electron–phonon coupling via Fröhlich interaction in the $Cs_2AgBiCl_6$ crystal. As the pressure increases, the E_{Stokes} decreases gradually, as evidenced by a negative shift of emission, as well as a continuous increase in the LO phonon mode energy. Therefore, the Huang–Rhys parameter decreases as a function of pressure, yielding a small value of about 8.5 at 4.5 GPa (Figure S11). This result shows that the electron–phonon coupling can be considerably reduced by lattice compression in the cubic phase.

Our mechanistic studies indicate that the broad emission of $Cs_2AgBiCl_6$ is primarily a result of exciton self-trapping due to strong coupling between the exciton and lattice. In addition, previous reports that self-trapped exciton (STE) emission in binary alkali halides shifts inversely with respect to the absorption edge upon compression is consistent with our emission mechanism.[44−47] The Jahn–Teller distortion, B-site metal disordering associated with the antisite defects [Bi_{Ag} (Bi-on-Ag) and Ag_{Bi} (Ag-on-Bi)], and a low electronic dimensionality are responsible for STE formation, which can result in localization through elastic lattice distortions and plays an important role in enhancing electron–phonon coupling.[13,18,48] Therefore, the stabilized and distorted excited trap states with a distribution of energy level relative to the ground state leads to a broad emission with a relatively large Stokes shift (Figure 5a).

Within the cubic phase of $Cs_2AgBiCl_6$, the blue shift of STE emission is mainly attributed to the reduced lattice relaxation energy E_{LR} with the contracted bond lengths and unchanged Br–Bi–Br and Br–Ag–Br bong angles, suggesting that the STE state of $Cs_2AgBiCl_6$ tends to a metastable state due to the electron–phonon coupling decrease.[45,49] The E_{LR} is related to the fwhm (Δ) of STE emission, $\Delta \propto \sqrt{2E_{LR}k_BT}$, which indicates that the E_{LR} decreases as pressure increases in the cubic phase.[47] The pressure effect of the activation energy barrier for self-trapping $E_{a,trap}$ and the potential barrier $E_{p,b}$ between adjacent STE state levels significantly affect the width and intensity of the emission band.[45,46,50] At ambient conditions, the carriers with constant lattice thermal energy surmount the activation barrier $E_{a,trap}$ or $E_{a,detrap}$ to realize the transition of exciton states from the free-exciton (FE) states to the STE states or from the STE states to the FE states. With increasing pressure, both the activation energy barrier for self-trapping $E_{a,trap}$ and the potential barrier $E_{p,b}$ gradually increase. The enhanced potential barrier $E_{p,b}$ with an adiabatic potential energy surface that changes from initially smooth to sharp causes STE localization. Thus, the emission band that we observed narrows and increases in intensity at lower pressures. The enhanced activation energy barrier $E_{a,trap}$ reduces FE with definite lattice thermal energy from the FE states into the STE states, thereby resulting in a continuous decrease in the emission intensity as pressure increases. The potential barrier $E_{p,b}$ is more sensitive to pressure change than the activation energy barrier $E_{a,trap}$; therefore, the STE first emission increases and then decreases with pressure. The overall STE evolution mechanisms are illustrated in Figure 5. The suppression effect of pressure on emission also contributes to the disappearance of the emission band, which is common in 3D metal halide perovskites.[36] The red shift of the band gap is due to the homogeneous reduction in octahedral volume, where Ag–Cl and Bi–Cl bond contraction enhances metal halide orbital coupling and electronic band dispersion.[26] For the tetragonal phase of $Cs_2AgBiCl_6$, the rotation and distortion of $AgCl_6$ and $BiCl_6$ octahedra increase the electron–phonon coupling strength, leading to emission red shift and broadening from about 5 to 7.5 GPa. Significantly enhancing electron–phonon coupling by increasing structural distortion has been confirmed in our recent low-dimensional metal halide perovskite studies.[51,52] Here, the rotation and distortion of $AgCl_6$ and $BiCl_6$ octahedra can decrease orbital coupling and electronic band dispersion and consequently decrease the band gap. The sharp increase of the band gap during the phase transition is likely dominated by the remarkable octahedra rotation from 5 to 7 GPa. The re-emergence of a decrease with further

DOI: 10.1021/acsenergylett.9b02155
ACS Energy Lett. 2019, 4, 2975−2982

compression suggests that Ag−Cl and Bi−Cl bond contractions bring about a stronger effect than octahedra rotation and distortion. With the increase in structural distortion, these two competing effects on the electronic landscape reach a balance, resulting in a nearly unchanged band gap over a large pressure range.

In summary, we studied the structural, optical, and electrical property changes in metal halide double perovskite $Cs_2AgBiCl_6$ upon compression up to 31 GPa at room temperature. The broad emission with a large Stokes shift is ascribed to exciton self-trapping due to strong electron−phonon coupling. Within the cubic phase, an abnormal PL blue shift accompanied by an absorption edge red shift occurs under pressure, which originates from the decreased lattice relaxation energy E_{LR} and increased metal halide orbital overlap upon Ag−Cl and Bi−Cl bond contraction, respectively. Octahedral rotation along the *c* axis leads to a structural phase transition from *Fm*-3*m* to *I*4/*m*, corresponding to a PL red shift and absorption edge blue shift. Strong electron−phonon coupling via Fröhlich interactions in $Cs_2AgBiCl_6$ is confirmed by the large Huang−Rhys parameter of 18.1. Lattice compression can effectively reduce the electron−phonon coupling strength in the cubic phase, which is our first discovery in the high-pressure studies of the 3D halide perovskites. Maintaining a highly symmetric cubic structure is crucial for achieving simultaneous band gap narrowing, electron−phonon coupling reduction, and ionic suppression under pressure. This work provides opportunities for the modulation and tuning of optical and electric transport properties of halide double perovskites and demonstrates the need for further exploration for improving their photovoltaic and optoelectronic performance by introducing lattice strain and chemical or mechanical pressure under practical conditions.

■ ASSOCIATED CONTENT

Supporting Information

The Supporting Information is available free of charge on the ACS Publications website at DOI: 10.1021/acsenergylett.9b02155.

Experimental details and additional figures and tables, showing absorption spectra, PL spectra, TRPL spectra, a pressure dependence plot, chromaticity coordinates, PL peak locations, synchrotron XRD patterns, inorganic frameworks, the evolution of cell parameters and volumes upon compression, Raman spectra, electrical resistance, evolution of the Huang−Rhys parameters, and SEM images (PDF)

■ AUTHOR INFORMATION

Corresponding Authors

*E-mail: kaiwang@jlu.edu.cn.
*E-mail: zoubo@jlu.edu.cn.

ORCID

Kai Wang: 0000-0003-4721-6717
Kaijun Yuan: 0000-0002-5108-8984
Bo Zou: 0000-0002-3215-1255

Notes

The authors declare no competing financial interest.

■ ACKNOWLEDGMENTS

This work was supported by the National Natural Science Foundation of China (NSFC) (No. 21725304, 11774120, and 21673100), the Chang Jiang Scholars Program of China (No. T2016051), and the fundamental research funds for the Central Universities. J.Y. and W.M. were supported by the U.S. Department of Energy, Office of Science, Basic Energy Sciences, Materials Sciences and Engineering Division (DE-AC02-76SF00515). This work was mainly performed at 4W2 HP-Station, Beijing Synchrotron Radiation Facility (BSRF). Portions of this work were performed at the BL15U1 at the Shanghai Synchrotron Radiation Facility (SSRF).

■ REFERENCES

(1) Eperon, G. E.; Leijtens, T.; Bush, K. A.; Prasanna, R.; Green, T.; Wang, J. T.-W.; McMeekin, D. P.; Volonakis, G.; Milot, R. L.; May, R.; et al. Perovskite-Perovskite Tandem Photovoltaics with Optimized Band Gaps. *Science* **2016**, *354*, 861−865.

(2) Jeon, N. J.; Noh, J. H.; Yang, W. S.; Kim, Y. C.; Ryu, S.; Seo, J.; Seok, S. I. Compositional Engineering of Perovskite Materials for High-Performance Solar Cells. *Nature* **2015**, *517*, 476−480.

(3) Tsai, H.; Nie, W.; Blancon, J. C.; Stoumpos, C. C.; Asadpour, R.; Harutyunyan, B.; Neukirch, A. J.; Verduzco, R.; Crochet, J. J.; Tretiak, S.; et al. High-Efficiency Two-Dimensional Ruddlesden-Popper Perovskite Solar Cells. *Nature* **2016**, *536*, 312−316.

(4) Correa-Baena, J.-P.; Saliba, M.; Buonassisi, T.; Grätzel, M.; Abate, A.; Tress, W.; Hagfeldt, A. Promises and Challenges of Perovskite Solar Cells. *Science* **2017**, *358*, 739−744.

(5) Rong, Y.; Hu, Y.; Mei, A.; Tan, H.; Saidaminov, M. I.; Seok, S. I.; McGehee, M. D.; Sargent, E. H.; Han, H. Challenges for Commercializing Perovskite Solar Cells. *Science* **2018**, *361*, No. eaat8235.

(6) Slavney, A. H.; Hu, T.; Lindenberg, A. M.; Karunadasa, H. I. A Bismuth-Halide Double Perovskite with Long Carrier Recombination Lifetime for Photovoltaic Applications. *J. Am. Chem. Soc.* **2016**, *138*, 2138−2141.

(7) McClure, E. T.; Ball, M. R.; Windl, W.; Woodward, P. M. Cs_2AgBiX_6(X = Br, Cl): New Visible Light Absorbing, Lead-Free Halide Perovskite Semiconductors. *Chem. Mater.* **2016**, *28*, 1348−1354.

(8) Yang, B.; Chen, J.; Yang, S.; Hong, F.; Sun, L.; Han, P.; Pullerits, T.; Deng, W.; Han, K. Lead-Free Silver-Bismuth Halide Double Perovskite Nanocrystals. *Angew. Chem., Int. Ed.* **2018**, *57*, 5359−5363.

(9) Yang, B.; Mao, X.; Hong, F.; Meng, W.; Tang, Y.; Xia, X.; Yang, S.; Deng, W.; Han, K. Lead-Free Direct Bandgap Double Perovskite Nanocrystals with Bright Dual-Color Emission. *J. Am. Chem. Soc.* **2018**, *140*, 17001−17006.

(10) Du, K. Z.; Meng, W.; Wang, X.; Yan, Y.; Mitzi, D. B. Bandgap Engineering of Lead-Free Double Perovskite $Cs_2AgBiBr_6$ through Trivalent Metal Alloying. *Angew. Chem., Int. Ed.* **2017**, *56*, 8158−8162.

(11) Steele, J. A.; Pan, W.; Martin, C.; Keshavarz, M.; Debroye, E.; Yuan, H.; Banerjee, S.; Fron, E.; Jonckheere, D.; Kim, C. W.; et al. Photophysical Pathways in Highly Sensitive $Cs_2AgBiBr_6$ Double-Perovskite Single-Crystal X-Ray Detectors. *Adv. Mater.* **2018**, *30*, 1804450.

(12) Pan, W.; Wu, H.; Luo, J.; Deng, Z.; Ge, C.; Chen, C.; Jiang, X.; Yin, W.-J.; Niu, G.; Zhu, L.; et al. $Cs_2AgBiBr_6$ Single-Crystal X-Ray Detectors with a Low Detection Limit. *Nat. Photonics* **2017**, *11*, 726−732.

(13) Luo, J.; Wang, X.; Li, S.; Liu, J.; Guo, Y.; Niu, G.; Yao, L.; Fu, Y.; Gao, L.; Dong, Q.; et al. Efficient and Stable Emission of Warm-White Light from Lead-Free Halide Double Perovskites. *Nature* **2018**, *563*, 541−545.

(14) Zhou, L.; Xu, Y. F.; Chen, B. X.; Kuang, D. B.; Su, C. Y. Synthesis and Photocatalytic Application of Stable Lead-Free $Cs_2AgBiBr_6$ Perovskite Nanocrystals. *Small* **2018**, *14*, 1703762.

DOI: 10.1021/acsenergylett.9b02155
ACS Energy Lett. 2019, 4, 2975−2982

(15) Greul, E.; Petrus, M. L.; Binek, A.; Docampo, P.; Bein, T. Highly Stable, Phase Pure $Cs_2AgBiBr_6$ Double Perovskite Thin Films for Optoelectronic Applications. *J. Mater. Chem. A* **2017**, *5*, 19972−19981.
(16) Pantaler, M.; Cho, K. T.; Queloz, V. I. E.; García Benito, I.; Fettkenhauer, C.; Anusca, I.; Nazeeruddin, M. K.; Lupascu, D. C.; Grancini, G. Hysteresis-Free Lead-Free Double-Perovskite Solar Cells by Interface Engineering. *ACS Energy Lett.* **2018**, *3*, 1781−1786.
(17) Ning, W.; Wang, F.; Wu, B.; Lu, J.; Yan, Z.; Liu, X.; Tao, Y.; Liu, J. M.; Huang, W.; Fahlman, M.; et al. Long Electron-Hole Diffusion Length in High-Quality Lead-Free Double Perovskite Films. *Adv. Mater.* **2018**, *30*, 1706246.
(18) Steele, J. A.; Puech, P.; Keshavarz, M.; Yang, R.; Banerjee, S.; Debroye, E.; Kim, C. W.; Yuan, H.; Heo, N. H.; Vanacken, J.; et al. Giant Electron-Phonon Coupling and Deep Conduction Band Resonance in Metal Halide Double Perovskite. *ACS Nano* **2018**, *12*, 8081−8090.
(19) Kentsch, R.; Scholz, M.; Horn, J.; Schlettwein, D.; Oum, K.; Lenzer, T. Exciton Dynamics and Electron-Phonon Coupling Affect the Photovoltaic Performance of the $Cs_2AgBiBr_6$ Double Perovskite. *J. Phys. Chem. C* **2018**, *122*, 25940−25947.
(20) Wright, A. D.; Verdi, C.; Milot, R. L.; Eperon, G. E.; Perez-Osorio, M. A.; Snaith, H. J.; Giustino, F.; Johnston, M. B.; Herz, L. M. Electron-Phonon Coupling in Hybrid Lead Halide Perovskites. *Nat. Commun.* **2016**, *7*, 11755.
(21) Zhu, X. Y.; Podzorov, V. Charge Carriers in Hybrid Organic-Inorganic Lead Halide Perovskites Might Be Protected as Large Polarons. *J. Phys. Chem. Lett.* **2015**, *6*, 4758−4761.
(22) Hoye, R. L. Z.; Eyre, L.; Wei, F.; Brivio, F.; Sadhanala, A.; Sun, S.; Li, W.; Zhang, K. H. L.; MacManus-Driscoll, J. L.; Bristowe, P. D.; et al. Fundamental Carrier Lifetime Exceeding 1 μs in $Cs_2AgBiBr_6$ Double Perovskite. *Adv. Mater. Interfaces* **2018**, *5*, 1800464.
(23) Volonakis, G.; Filip, M. R.; Haghighirad, A. A.; Sakai, N.; Wenger, B.; Snaith, H. J.; Giustino, F. Lead-Free Halide Double Perovskites Via Heterovalent Substitution of Noble Metals. *J. Phys. Chem. Lett.* **2016**, *7*, 1254−1259.
(24) Schade, L.; Wright, A. D.; Johnson, R. D.; Dollmann, M.; Wenger, B.; Nayak, P. K.; Prabhakaran, D.; Herz, L. M.; Nicholas, R.; Snaith, H. J.; et al. Structural and Optical Properties of $Cs_2AgBiBr_6$ Double Perovskite. *ACS Energy Lett.* **2019**, *4*, 299−305.
(25) Zhang, L.; Liu, C.; Wang, L.; Liu, C.; Wang, K.; Zou, B. Pressure-Induced Emission Enhancement, Band-Gap Narrowing, and Metallization of Halide Perovskite $Cs_3Bi_2I_9$. *Angew. Chem., Int. Ed.* **2018**, *57*, 11213−11217.
(26) Kong, L.; Liu, G.; Gong, J.; Hu, Q.; Schaller, R. D.; Dera, P.; Zhang, D.; Liu, Z.; Yang, W.; Zhu, K.; et al. Simultaneous Band-Gap Narrowing and Carrier-Lifetime Prolongation of Organic-Inorganic Trihalide Perovskites. *Proc. Natl. Acad. Sci. U. S. A.* **2016**, *113*, 8910−8915.
(27) Yin, T.; Fang, Y.; Chong, W. K.; Ming, K. T.; Jiang, S.; Li, X.; Kuo, J. L.; Fang, J.; Sum, T. C.; White, T. J.; et al. High-Pressure-Induced Comminution and Recrystallization of CH_3NH_3 $PbBr_3$ Nanocrystals as Large Thin Nanoplates. *Adv. Mater.* **2018**, *30*, 1705017.
(28) Lu, X.; Wang, Y.; Stoumpos, C. C.; Hu, Q.; Guo, X.; Chen, H.; Yang, L.; Smith, J. S.; Yang, W.; Zhao, Y.; et al. Enhanced Structural Stability and Photo Responsiveness of $CH_3NH_3SnI_3$ Perovskite Via Pressure-Induced Amorphization and Recrystallization. *Adv. Mater.* **2016**, *28*, 8663−8668.
(29) Wang, Y.; Lu, X.; Yang, W.; Wen, T.; Yang, L.; Ren, X.; Wang, L.; Lin, Z.; Zhao, Y. Pressure-Induced Phase Transformation, Reversible Amorphization and Anomalous Visible Light Response in Organolead Bromide Perovskite. *J. Am. Chem. Soc.* **2015**, *137*, 11144−11149.
(30) Zhu, H.; Cai, T.; Que, M.; Song, J. P.; Rubenstein, B. M.; Wang, Z.; Chen, O. Pressure-Induced Phase Transformation and Band-Gap Engineering of Formamidinium Lead Iodide Perovskite Nanocrystals. *J. Phys. Chem. Lett.* **2018**, *9*, 4199−4205.
(31) Jiang, S.; Luan, Y.; Jang, J. I.; Baikie, T.; Huang, X.; Li, R.; Saouma, F. O.; Wang, Z.; White, T. J.; Fang, J. Phase Transitions of Formamidinium Lead Iodide Perovskite under Pressure. *J. Am. Chem. Soc.* **2018**, *140*, 13952−13957.
(32) Wang, T.; Daiber, B.; Frost, J. M.; Mann, S. A.; Garnett, E. C.; Walsh, A.; Ehrler, B. Indirect to Direct Bandgap Transition in Methylammonium Lead Halide Perovskite. *Energy Environ. Sci.* **2017**, *10*, 509−515.
(33) Jaffe, A.; Lin, Y.; Mao, W. L.; Karunadasa, H. I. Pressure-Induced Metallization of the Halide Perovskite $(CH_3NH_3)PbI_3$. *J. Am. Chem. Soc.* **2017**, *139*, 4330−4333.
(34) Liu, G.; Gong, J.; Kong, L.; Schaller, R. D.; Hu, Q.; Liu, Z.; Yan, S.; Yang, W.; Stoumpos, C. C.; Kanatzidis, M. G.; et al. Isothermal Pressure-Derived Metastable States in 2d Hybrid Perovskites Showing Enduring Bandgap Narrowing. *Proc. Natl. Acad. Sci. U. S. A.* **2018**, *115*, 8076−8081.
(35) Li, Q.; Wang, Y.; Pan, W.; Yang, W.; Zou, B.; Tang, J.; Quan, Z. High Pressure Band Gap Engineering in Lead-Free $Cs_2AgBiBr_6$ Double Perovskite. *Angew. Chem., Int. Ed.* **2017**, *56*, 15969.
(36) Jaffe, A.; Lin, Y.; Beavers, C. M.; Voss, J.; Mao, W. L.; Karunadasa, H. I. High-Pressure Single-Crystal Structures of 3D Lead-Halide Hybrid Perovskites and Pressure Effects on Their Electronic and Optical Properties. *ACS Cent. Sci.* **2016**, *2*, 201−209.
(37) Wang, Z.; Schliehe, C.; Wang, T.; Nagaoka, Y.; Cao, Y. C.; Bassett, W. A.; Wu, H.; Fan, H.; Weller, H. Deviatoric Stress Driven Formation of Large Single-Crystal PbS Nanosheet from Nanoparticles and in Situ Monitoring of Oriented Attachment. *J. Am. Chem. Soc.* **2011**, *133*, 14484−14487.
(38) Wang, Z.; Finkelstein, K.; Ma, C.; Wang, Z. L. Structure Stability, Fracture, and Tuning Mechanism of CdSe Nanobelts. *Appl. Phys. Lett.* **2007**, *90*, 113115.
(39) Wang, P.; Guan, J.; Galeschuk, D. T. K.; Yao, Y.; He, C. F.; Jiang, S.; Zhang, S.; Liu, Y.; Jin, M.; Jin, C.; et al. Pressure-Induced Polymorphic, Optical, and Electronic Transitions of Formamidinium Lead Iodide Perovskite. *J. Phys. Chem. Lett.* **2017**, *8*, 2119−2125.
(40) Szafranski, M.; Katrusiak, A. Mechanism of Pressure-Induced Phase Transitions, Amorphization, and Absorption-Edge Shift in Photovoltaic Methylammonium Lead Iodide. *J. Phys. Chem. Lett.* **2016**, *7*, 3458−3466.
(41) Yan, H.; Ou, T.; Jiao, H.; Wang, T.; Wang, Q.; Liu, C.; Liu, X.; Han, Y.; Ma, Y.; Gao, C. Pressure Dependence of Mixed Conduction and Photo Responsiveness in Organolead Tribromide Perovskites. *J. Phys. Chem. Lett.* **2017**, *8*, 2944−2950.
(42) Yang, B.; Pan, W.; Wu, H.; Niu, G.; Yuan, J. H.; Xue, K. H.; Yin, L.; Du, X.; Miao, X. S.; Yang, X.; et al. Heteroepitaxial Passivation of $Cs_2AgBiBr_6$ Wafers with Suppressed Ionic Migration for X-ray Imaging. *Nat. Commun.* **2019**, *10*, 1989.
(43) de Jong, M.; Seijo, L.; Meijerink, A.; Rabouw, F. T. Resolving the Ambiguity in the Relation between Stokes Shift and Huang-Rhys Parameter. *Phys. Chem. Chem. Phys.* **2015**, *17*, 16959−16969.
(44) Kobayashi, M.; Ohno, Y.; Endo, S.; Cho, K.; Narita, S. Instability of Self-Trapped Exciton Caused by Hydrostatic Pressure in AgCl. *Physica B+C* **1983**, *117-118*, 272−274.
(45) Tsujimoto, T.; Nishimura, H.; Nakayama, M. Hydrostatic Pressure Effects on the Free and Self-Trapped Exciton States in Csi. *Phys. Rev. B: Condens. Matter Mater. Phys.* **1996**, *54*, 16579−16584.
(46) Nishimura, H.; Tsujimoto, T.; Nakayama, M.; Morita, S.; Kobayashi, M. Spectral Changes of the Self-Trapped Exciton Luminescence in RbI under Hydrostatic Pressure. *J. Lumin.* **1994**, *62*, 41−47.
(47) Saitoh, A.; Komatsu, T.; Karasawa, T. Exciton-Phonon Interaction and Conversion of Excitons from Free to Self-Trapped States in Layered Metal Iodide Crystals under Hydrostatic Pressure. *J. Lumin.* **2000**, *87*, 633−635.
(48) Wang, X.; Meng, W.; Liao, W. Q.; Wang, J.; Xiong, R. G.; Yan, Y. Atomistic Mechanism of Broadband Emission in Metal Halide Perovskites. *J. Phys. Chem. Lett.* **2019**, *10*, 501−506.
(49) Kobayashi, M.; Hirose, T.; Nishimura, H. High Pressure Effects on Self-Trapped Excitons in RbI. *J. Lumin.* **1991**, *48*, 98−102.

DOI: 10.1021/acsenergylett.9b02155
ACS Energy Lett. 2019, 4, 2975−2982

(50) Kurisu, H.; Komatsu, T.; Karasawa, T. Hydrostatic Pressure Effects on the Excitons and Exciton-Phonon Interaction in BiI_3 Crystals. *J. Phys. Soc. Jpn.* **1993**, *62*, 1048−1056.
(51) Zhang, L.; Wu, L.; Wang, K.; Zou, B. Pressure-Induced Broadband Emission of 2D Organic-Inorganic Hybrid Perovskite $(C_6H_5C_2H_4NH_3)_2PbBr_4$. *Adv. Sci.* **2019**, *6*, 1801628.
(52) Ma, Z.; Liu, Z.; Lu, S.; Wang, L.; Feng, X.; Yang, D.; Wang, K.; Xiao, G.; Zhang, L.; Redfern, S. A. T.; et al. Pressure-Induced Emission of Cesium Lead Halide Perovskite Nanocrystals. *Nat. Commun.* **2018**, *9*, 4506.

DOI: 10.1021/acsenergylett.9b02155
ACS Energy Lett. 2019, 4, 2975−2982